J. Fluid Mech. (1994), *vol.* 273, *pp.* 285–312

Evolution and breakup of vortex rings in straining and shearing flows

By J. S. MARSHALL[1] AND J. R. GRANT[2]

[1] Iowa Institute of Hydraulic Research, The University of Iowa, Iowa City, IA 52242, USA

[2] Naval Undersea Warfare Center, Newport, RI 02841, USA

(Received 8 October 1992 and in revised form 18 February 1994)

A study of the effect of external straining and shearing flows on the evolution and form of breakup of vortex rings has been performed. Two orientations each of straining and shearing flows are considered. A theoretical analysis of the ring motion for small strain and shear rates is performed, and it is found that for shearing and straining flows in the plane of the ring, the ring may oscillate periodically. For a straining flow with compression normal to the initial plane of the ring, the linear theory predicts that the ring radius will expand with time. For shearing flow normal to the initial plane of the ring, the linear theory predicts tilting of the ring in the direction of the shear flow rotation.

Numerical calculations are performed with both single vortex filaments and with a three-dimensional discrete vortex element method. The numerical calculations confirm the predictions of the linear theory for values of strain and shear rates below a certain critical value (which depends on the ratio R/σ_0 of initial ring to core radii), whereas for strain and shear rates above this value the ring becomes very elongated with time and eventually pinches off. Three distinct regimes of long-time behaviour of the ring have been identified. Regime selection depends on initial ring geometry and orientation and on values of strain and shear rates. These regimes include (i) periodic oscillations with no pinching off, (ii) pinching off at the ring centre, and (iii) development of an elongated vortex pair at the ring centre and wider 'heads' near the ends (with pinching off just behind the heads). The boundaries of these regimes and theoretical reasons for the vortex behaviour in each case are described. It is also shown that the breakup of stretched vortex rings exhibits a self-similar behaviour, in which the number and size of 'offspring' vortices, at the point of pinching-off the ring, may be scaled by the product of the strain rate e (or shear rate s) and the oscillation period τ of a slightly elliptical ring with mean radius R.

1. Introduction

There has been a great amount of recent interest in problems involving reconnection of vortex filaments and the breakup of vortex structures. For instance, a number of recent investigations have been made of the collision of two or more vortex structures, and in particular of vortex rings (e.g. Kida, Takaoka & Hussain 1991), and the subsequent breakup and reformation of the rings. Vortex structures may also break up owing to their own self-induced velocity, and the processes leading to breakup in these instances have been somewhat less studied. One example of such a process was demonstrated by Dhanak & Bernardinis (1981), who showed that an isolated, initially elliptical vortex ring can either undergo a periodic (or nearly periodic) oscillatory

motion or it can pinch off on itself (thus forming two rings), depending on the initial value of the ring aspect ratio.

In the present paper, we examine the evolution and breakup of initially circular vortex rings which are subject to external straining or shearing flows. We find that under certain conditions the ring may achieve a periodic (or nearly periodic) oscillation, but that when these conditions are not satisfied the ring pinches off on itself. However, the pinching off is found to adopt a variety of forms depending on the initial geometry and orientation of the ring and the strain and shear rates. Of particular note, our results indicate that a vortex ring may break up to form 'offspring' of unequal size and energy and that more than two offspring may result from the ring breakup. In fact, the results of the paper indicate a self-similarity in breakup of the ring that allows one to easily predict the sizes and form of the offspring. These features of vortex ring breakup which are demonstrated in the paper may have some relevance to development of multiplicative models of turbulent energy cascade, such as have been discussed by Mandelbrot (1974), Frisch, Sulem & Nelkin (1978) and Meneveau & Sreenivasan (1987, 1991). However, application of the present work to these and other problems is also restricted in the sense that the initial condition for the current analysis is always a circular vortex ring, and it is an open question whether solutions for such a configuration are at all indicative of the behaviour and breakup of more general classes of vortex structures in straining or shearing flows. A number of other applications of vortex rings in industrial processes, acoustics and environmental problems, to which the present results would be relevant, are described in the recent review by Shariff & Leonard (1992).

The paper uses three approaches, one theoretical and two computational, to solve for various aspects of the ring evolution when immersed in external straining and shearing flows. The first computational approach, which employs a model of the ring in the form of a single vortex filament that admits waves of variable core area along the vortex axis, is described in §2 along with a statement of the specific problem geometry. The evolution of the ring for small strain and shear rates is then analysed using a linear theory in §3. In §§4–7, we describe the results of the single filament computations for the nonlinear ring evolution. In §8, an alternative computational approach is presented using the three-dimensional discrete vortex element (DVE) algorithm of Knio & Ghoniem (1990). These DVE calculations are used both to examine the accuracy of and to extend the single filament computations for cases with an external straining flow. Cases involving reconnection or 'collapse' of the vortex cores and others involving local instability of the cores to the external flow are examined with the DVE computations. Some conclusions from the study are given in §9.

2. Description of the vortex model and solution procedure

In this paper, we consider the evolution of an initially circular vortex ring subject to a straining or shearing flow. An illustration of the four initial configurations considered in the paper is shown in figure 1 for external straining flows and in figure 2 for external shearing flows. For straining flows, these configurations include cases where the directions of both straining and compression lie in the initial plane of the vortex ring (called the 'in-plane straining' case) and cases where the direction of compression is normal to the initial plane of the ring (called the 'normal straining' case). For shearing flows, configurations are considered where the direction of the shear flow is in the initial plane of the ring (called the 'in-plane shearing' case) and where the shear flow

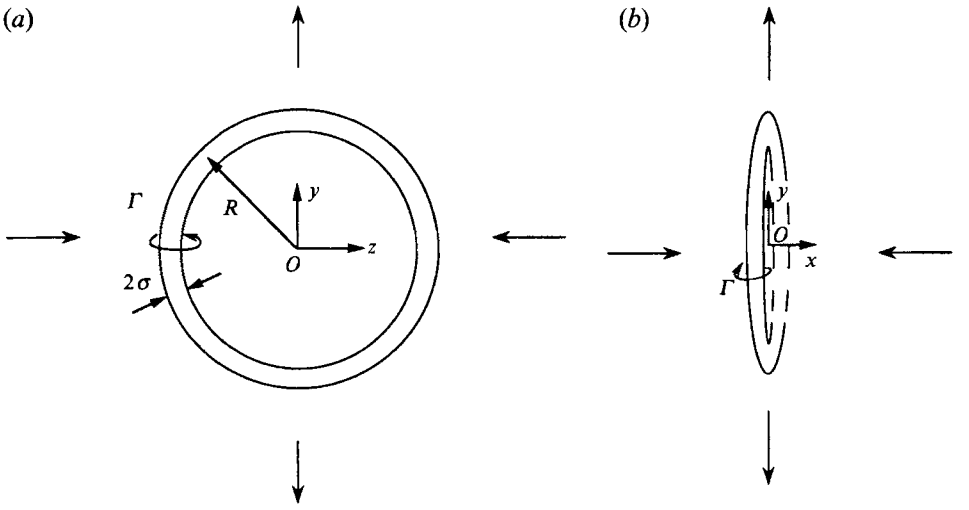

FIGURE 1. Schematic of the initial configurations of the vortex rings for the case of external straining flow. In the in-plane straining (PST) case shown in (*a*), the directions of both stretching and compression lie in the initial plane of the ring. In the normal straining (NST) case shown in (*b*), the direction of compression is normal to the initial plane of the ring.

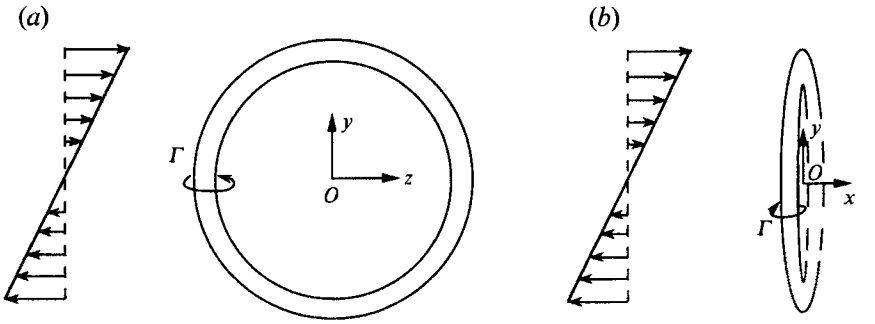

FIGURE 2. Schematic of the initial configurations of the vortex ring for the case of external shearing flow. In the in-plane shearing (PSH) case shown in (*a*), the direction of external flow is in the initial plane of the ring. In the normal shearing (NSH) case shown in (*b*), the direction of external flow is normal to the initial plane of the ring.

is normal to the initial plane of the ring (called the 'normal shearing' case). In order to facilitate reference to these various configurations in the remainder of the paper, we introduce acronyms in which the first letter, P or N, indicates whether the flow acts in the plane or normal to the plane of the ring and the second two letters, ST or SH, denote whether the flow is of the plane-strain or shearing type, respectively. Thus, the configurations in figures 1 (*a*), 1 (*b*), 2 (*a*) and 2 (*b*) are referred to as PST, NST, PSH and NSH, respectively. A Cartesian coordinate system is shown in figures 1 and 2 such that the axis C of the ring initially coincides with a circle of radius R in the (y, z)-plane, and the vortex circulation Γ is such that the ring will initially propagate in the positive x-direction. For straining flows, the direction of stretching is always chosen to coincide with the y-axis, whereas compression may occur along either the x-axis (NST) or the z-axis (PST). In the case of shearing flows, the flow direction is in the (y, z)-plane for PSH and in the (x, y)-plane for NSH.

The evolution of the ring with time is solved for using a modified form of the so-called cutoff model (Moore & Saffman 1972) which admits axial wave motion on the vortex core. In this relatively simple model, the ring is represented by a single filament that is convected by the sum of three velocity fields: (i) the self-induced velocity $\boldsymbol{u}_B$ of the ring, (ii) the external straining or shearing flow $\boldsymbol{u}_E$ and (iii) an axial velocity $w\boldsymbol{\lambda}_3$, where $\boldsymbol{\lambda}_3$ is the unit tangent to C at time t and w is the axial velocity within the vortex core relative to the flow just outside the core. We let ξ denote the angle in the initial plane that coincides with some arbitrary point P on the ring axis C, where for definiteness we set $\xi = 0$ on the positive z-axis. The parameter ξ can thus be used to identify material points on the ring axis. If $\boldsymbol{r}(t, \xi)$ is the position vector to some point on the ring axis C at time t, the motion of the ring is determined by

$$\frac{\mathrm{d}\boldsymbol{r}}{\mathrm{d}t} = \boldsymbol{u}_B + \boldsymbol{u}_E + w\boldsymbol{\lambda}_3, \tag{1}$$

where the external flow is given for the four configurations shown in figures 1 and 2 by

$$\boldsymbol{u}_E = \begin{cases} ey\boldsymbol{e}_y - ez\boldsymbol{e}_z & \text{in PST,} \\ ey\boldsymbol{e}_y - ex\boldsymbol{e}_x & \text{in NST,} \\ sy\boldsymbol{e}_z & \text{in PSH,} \\ sy\boldsymbol{e}_x & \text{in NSH.} \end{cases} \tag{2}$$

Here e is the strain rate, s is the shear rate, $\mathrm{d}/\mathrm{d}t$ is the total derivative (keeping ξ fixed) and $(\boldsymbol{e}_x, \boldsymbol{e}_y, \boldsymbol{e}_z)$ are base vectors in the x-, y- and z-directions.

The self-induced velocity $\boldsymbol{u}_B$ at some point ξ_0 on C is obtained from the Biot–Savart integral, with a Rosenhead cutoff to avoid the singularity, as

$$\boldsymbol{u}_B(\xi_0, t) = \frac{\Gamma}{4\pi} \int_C \frac{\partial \boldsymbol{r}}{\partial \xi}(\xi, t) \times \frac{(\boldsymbol{r}(\xi_0, t) - \boldsymbol{r}(\xi, t))}{[|\boldsymbol{r}(\xi_0, t) - \boldsymbol{r}(\xi, t)|^2 + \mu^2(\xi_0, t)]^{3/2}} \mathrm{d}\xi. \tag{3}$$

The parameter μ, which is added to the denominator in (3) in order to avoid the singularity at $\xi = \xi_0$, is proportional to the core radius $\sigma(\xi_0, t)$ and is given by $\mu = 2\delta_R \sigma$. The constant δ_R is related to the vorticity profile in the vortex core (Moore & Saffman 1972; Dhanak & Bernardinis 1981) by

$$\ln(2\delta_R) = -\tfrac{1}{2} - A - \frac{4\pi^2 w^2 \sigma^2}{\Gamma^2}, \tag{4}$$

where if the azimuthal velocity within the vortex core is given by $v(r) = (\Gamma/2\pi r) f(r/\sigma)$, then the constant A is obtained as

$$A = \int_0^1 f^2(\eta) \frac{\mathrm{d}\eta}{\eta}. \tag{5}$$

In the present paper, we consider vortices with uniform vorticity across the core, for which case $A = \frac{1}{4}$.

The vortex core radius σ is obtained from the condition that the vortex core is a material region for an inviscid fluid. Let us define a vector $\boldsymbol{a}_3$ which is everywhere tangent to the ring axis C (but not necessarily of unit length) by $\boldsymbol{a}_3 = \partial \boldsymbol{r}/\partial \xi$, such that the magnitude of $\boldsymbol{a}_3$ is

$$(a_{33})^{1/2} = (\boldsymbol{a}_3 \cdot \boldsymbol{a}_3)^{1/2}. \tag{6}$$

The ratio of $(a_{33})^{1/2}$ at point ξ at any time t divided by the initial value of $(a_{33})^{1/2}$ at point ξ is equal to the stretch of an infinitesimal material line segment of length $\mathrm{d}s$ centred at ξ and lying along the ring axis C. From the condition that the core volume of each section of the vortex is conserved and the relationship $\mathrm{d}s = (a_{33})^{1/2}\,\mathrm{d}\xi$, it follows that the volume of fluid $\pi\sigma^2\,\mathrm{d}s$ contained in an infinitesimal material section of the core is constant. An expression for the change in core radius with time is then given by

$$\sigma(\xi, t) = \sigma(\xi, 0)\left\{\frac{|\partial \boldsymbol{r}(\xi, t)/\partial\xi|}{|\partial \boldsymbol{r}(\xi, 0)/\partial\xi|}\right\}^{1/2}. \tag{7}$$

The unit tangent vector $\boldsymbol{\lambda}_3$ to C is parallel to $\boldsymbol{a}_3$, so

$$\boldsymbol{\lambda}_3 = \boldsymbol{a}_3/(a_{33})^{1/2} = \frac{\partial \boldsymbol{r}}{\partial\xi}\Big/\left|\frac{\partial \boldsymbol{r}}{\partial\xi}\right|. \tag{8}$$

Since one part of the vortex core may undergo greater or lesser stretching from the external flow than another part of the core, differences in core radius may evolve over time. However, variation in core area produces an axial force on the core fluid which gives rise to an axial motion within the core that acts to restore the core to a state of nearly uniform cross-sectional area. Since the response of the core is quite fast to such axial motions, several previous studies (e.g. Moore & Saffman 1972; Dhanak & Bernardinis 1981) have simply restricted the core to be everywhere of uniform radius. We have adopted in this paper a somewhat less restrictive assumption and have instead allowed an internal axial core flow $w(\xi, t)$ to exist. (In our computations, however, the core radius is found not to differ by more than about 10% between different sections of the ring at any given time, and the results would not therefore have differed significantly had we simply required the core radius to be uniform.) The equation for w is obtained from the vortex axial momentum equation as a simplification of the theories of Lundgren & Ashurst (1989) or Marshall (1991) as

$$\frac{\mathrm{d}w}{\mathrm{d}t} = -\frac{\Gamma^2}{4\pi^2\sigma^3}\frac{\partial\sigma}{\partial s}. \tag{9}$$

Aside from a factor of $\pi\sigma^2$ times the fluid density, the left-hand side of (9) represents the rate of change of axial momentum due to motion along the core axis and the right-hand side represents the axial force on the core lateral surface. Equation (9) yields a solution for propagation speed of small-amplitude axisymmetric waves of variable core area on a vortex with ambient core radius σ_0 as $c = \Gamma/\sqrt{8\pi\sigma_0}$, which is of the same form as the expression given by Kelvin (1880) but the constant differs by about 15% owing to a difference in the assumed axial velocity profile. We note that the simple theory for vortex motion given in (1)–(9) can be obtained formally from the theories of Lundgren & Ashurst (1989) and Marshall (1991) using a multiple timescale perturbation method for small values of the parameter σ/L, where L is a typical lengthscale along the vortex axis. The derivation makes use of the observation that the timescale for axisymmetric wave motion on the core is less than that for lateral displacement of the core axis (say, in the form of helical waves) by a factor of σ/L to systematically eliminate the higher-order terms in the vortex momentum equations. For the modified cutoff theory developed by Moore & Saffman (1972), there is also an implicit assumption that the self-induced velocity of the vortex is in the binormal direction to the vortex axis. One advantage of using this simplified formulation for the evolution of the vortex filament is that reliable methods exist for numerical solution of equation (9) for w and equations (1)–(3) for the lateral displacement of the filament.

In the remainder of the paper, we non-dimensionalize all lengths by the core radius σ_0, all velocities by the maximum value $\Gamma/2\pi\sigma_0$ of the azimuthal velocity on the initial plane (assuming a 'thin' vortex ring in which $R/\sigma \gg 1$) and time by $\Gamma/2\pi\sigma_0^2$. The dimensionless versions of (1)–(9) governing the ring motion can be obtained simply by setting $\Gamma = 2\pi$ in these equations.

In the numerical solutions presented in §§4–7, the set of equations (1)–(9) for $\boldsymbol{r}(\xi, t)$ and $\sigma(\xi, t)$ are solved using a two-step predictor–corrector algorithm to advance in time. A three-point central difference is used for the derivative $\partial \boldsymbol{r}/\partial\xi$ in the Biot–Savart integral (3) and in determining σ and λ_3 from (7) and (8), and trapezoidal integration about the ring axis C is used to solve (3). Equation (9) for w is hyperbolic, so for purposes of numerical stability we have recast this equation in conservation form and solve it using MacCormack's scheme (see Peyret & Taylor 1983, p. 48), which is a second-order accurate scheme in which forward spatial differences are taken on the predictor step and backward spatial differences on the corrector step. Calculations were done with 400–800 equal increments about the ring axis, although various symmetry properties of the ring across the y- and z-axes were used to reduce computational time for problems involving external straining flows. The computations were performed on a Cray X-MP and typically required less than 30 min of CPU time, with timesteps Δt ranging from 0.05 to 0.1 depending on the problem under consideration. Select runs with smaller timesteps were used to verify that the results were independent of the value of Δt.

The dimensionless propagation speed c of a long axial wave on the core is approximately $0.11/\sigma$ (where we recall that the dimensionless core radius σ equals unity on the initial plane). The CFL condition then states that the numerical solution of (9) is stable (cf. Press *et al.* 1989) so long as $c\Delta t < \Delta s$, which for N segments about the ring axis implies that for stability we must choose Δt less than about $57.1\, R\sigma/N$. We typically selected Δt at about $\frac{1}{10}$ of this value.

In solving these equations, a numerical instability was found to occur after a long time which causes a jaggedness of the ring axis and eventually results in blowing up of the computations. This instability also occurs when we require σ to be uniform about the ring, only somewhat later. The instability was eliminated by smoothing the changes in $\boldsymbol{r}$ and w at every timestep using a spectral filter introduced by Orszag & Gottlieb (1980). This filter involves three steps: (i) the changes in $\boldsymbol{r}$ and w at time t are written as Fourier series with N terms (the other terms being truncated), (ii) the coefficient of the nth term in the Fourier series is multiplied by the factor f_n defined by

$$f_n = \frac{1-\exp[-(N^2-n^2)/N_0^2]}{1-\exp[-N^2/N_0^2]}, \tag{10}$$

where N_0 is an adjustable parameter which we set to $2N$, and (iii) the changes in $\boldsymbol{r}$ and w are recalculated from the truncated Fourier series. We usually took $N \approx 30$ in the computations, although variation of N for values over about 15 did not seem to affect the results very much.

Before leaving this section, we offer some discussion on the shortcomings of the simple model described above. One feature already mentioned is that the model applies only to inviscid flows (since the volume of core fluid is assumed to be conserved), so that diffusion of vorticity is neglected. Thus, the model will not reproduce the Burgers (1948) solution in which a balance is achieved between concentration of vorticity by stretching and diffusion of vorticity for a uniformly stretched vortex filament. Similarly, vorticity expulsion (Pearson & Abernathy 1984; Moore 1985) would not be predicted by the model for a diffusing line vortex with a shear flow along the vortex

axis. Secondly, the vortex core is assumed to be everywhere circular in the model, so that instabilities of the core in the presence of straining and shearing flows (Moore & Saffman 1971; Kida 1981; Neu 1984) would not be observed in the calculations. Thirdly, it is implicit in the derivation of this model (see Moore & Saffman 1972) that the product of axis curvature κ with core radius σ be small and that the separation distance L_s between two opposing sections of the ring (in a direction normal to C) be much larger than σ. Both of these assumptions are violated at various points of our computations.

The applicability of this model to flows with an external shear, as is the case in the configuration shown in figure 2, is also somewhat in question since the stretching of the background vorticity field by the vortex velocity field is not accounted for. A scaling argument was given by Aref & Flinchem (1984) which suggests that neglect of this effect is approximately valid if the typical lengthscale of the external shearing flow is much greater than the vortex core radius. In terms of the current dimensionless variables, this result implies the restriction $sR \ll 1$. In the current computations, the value of the product sR varies between about 0.2 and 0.5, so this restriction is only marginally satisfied.

3. Linear theory for small strain and shear rates

For cases in which the strain rate e or the shear rate s multiplied by the characteristic time τ of ring oscillation (in the axis-switching mode described by Dhanak & Bernadinis 1981) is small compared to unity, the ring remains nearly circular during several periods of oscillation. In fact, for some cases we will show that the ring will remain nearly circular indefinitely when $e\tau \ll 1$ or $s\tau \ll 1$, whereas in other cases the ring will become increasingly elongated in time for all values of $e\tau$ or $s\tau$. An analysis for nearly circular vortex rings is given in this section, which is an extension of the linear stability theory for vortex rings by Widnall & Sullivan (1973) and is based on the vortex model described in §2.

We write the position $\boldsymbol{r}(\xi, t)$ of the ring axis C at time t in terms of the polar base vectors $\boldsymbol{e}_r = \cos(\xi)\,\boldsymbol{e}_y + \sin(\xi)\,\boldsymbol{e}_z$ and $\boldsymbol{e}_\xi = -\sin(\xi)\,\boldsymbol{e}_y + \cos(\xi)\,\boldsymbol{e}_z$ as

$$\boldsymbol{r}(\xi, t) = R^*(\xi)\,\boldsymbol{e}_r + X_C(t)\,\boldsymbol{e}_x + \frac{1}{2}\sum_{m=-M}^{M}\{\rho_m(t)\,\mathrm{e}^{\mathrm{i}m\xi}\boldsymbol{e}_r + \beta_m(t)\,\mathrm{e}^{\mathrm{i}m\xi}\boldsymbol{e}_\xi + \gamma_m(t)\,\mathrm{e}^{\mathrm{i}m\xi}\boldsymbol{e}_x\}, \quad (11)$$

where m indicates the mode and M is the number of modes under consideration. The functions $(\rho_m, \beta_m, \gamma_m)$ are in general complex, and it is understood that $(\rho_{-m}, \beta_{-m}, \gamma_{-m})$ are equal to the complex conjugates of $(\rho_m, \beta_m, \gamma_m)$, respectively. For the case of nearly circular rings, we define a small parameter ϵ by $\epsilon \equiv \sup|\rho_m/R|$ and require that $\epsilon \ll 1$ and that both β_m/R and γ_m/R are $O(\epsilon)$. The function R^* is independent of time and is assumed to differ from the initial ring radius R by at most a factor of $O(\epsilon)$, or $R^*(\xi) = R(1 + O(\epsilon))$. Use of a function R^* which differs slightly from the ring radius R in this term is useful for satisfying the initial conditions of the problem, as will be shown presently. The function $X_C(t)$ denotes the displacement of the mean ring position from the initial plane (where $X_C/R = O(1)$), and we define $U = \mathrm{d}X_C/\mathrm{d}t$ as the mean ring propagation speed. For the nearly circular case, the self-induced velocity was obtained by Widnall & Sullivan (1973) from the Biot–Savart integral to leading order in ϵ as

$$\boldsymbol{u}_B = U\boldsymbol{e}_x + \frac{1}{2}\sum_{m=-M}^{M}[C_m\,\gamma_m(t)\,\mathrm{e}^{\mathrm{i}m\xi}\boldsymbol{e}_r + D_m\,\rho_m(t)\,\mathrm{e}^{\mathrm{i}m\xi}\boldsymbol{e}_x], \quad (12)$$

where C_m and D_m are real constants which depend on the mode m of oscillation. For $R \gg 1$ (where we recall that lengths are non-dimensionalized by σ_0), the results of Widnall & Sullivan (1973) give

$$C_m = C_{-m} \sim -\frac{m^2}{2R^2}\ln(R), \quad D_m = D_{-m} \sim -\frac{1-m^2}{2R^2}\ln(R). \tag{13}$$

The expressions (13) are valid for the leading order $O(\ln(R))$ terms, but neglect the $O(1)$ terms.

The external flow to the ring, given by (2), may contain displacement of a material point on C in the r, x and ξ directions. Differences in displacements in the ξ direction about the ring cause a convergence or divergence of the core material, which result in variation in core area about the ring. We assume in this linear theory (and justify the assumption by nonlinear computations) that variation in core area caused by displacements in the ξ-direction from the external flow are resisted by the internal axial flow so as to make the core area nearly uniform for all time. On the basis of the assumption of constant core area, we ignore displacements in the ξ-direction in the linear theory. From (2) and the relationship between Cartesian and polar base vectors, we can write the r and x components of the external flow as follows:

$$\boldsymbol{u}_E \cdot \boldsymbol{e}_r = \begin{cases} e[R^* + (\tfrac{1}{2})\Sigma\rho_m \mathrm{e}^{\mathrm{i}m\xi}]\cos(2\xi) & \text{in PST,} \\ e[R^* + (\tfrac{1}{2})\Sigma\rho_m \mathrm{e}^{\mathrm{i}m\xi}]\cos^2(\xi) & \text{in NST,} \\ (s/2)[R^* + (\tfrac{1}{2})\Sigma\rho_m \mathrm{e}^{\mathrm{i}m\xi}]\sin(2\xi) & \text{in PSH,} \\ 0 & \text{in NSH,} \end{cases} \tag{14a}$$

and

$$\boldsymbol{u}_E \cdot \boldsymbol{e}_x = \begin{cases} 0 & \text{in PST,} \\ -e[X_C + (\tfrac{1}{2})\Sigma\gamma_m \mathrm{e}^{\mathrm{i}m\xi}] & \text{in NST,} \\ 0 & \text{in PSH,} \\ s[R^* + (\tfrac{1}{2})\Sigma\rho_m \mathrm{e}^{\mathrm{i}m\xi}]\cos(\xi) & \text{in NSH,} \end{cases} \tag{14b}$$

where Σ implies a sum over all modes from $m = -M$ to M.

Substituting (11)–(14) into the equation of motion (1) for the vortex filament and taking the components of the resulting equation in the r- and x-directions gives

$$\left.\begin{aligned} \frac{1}{2}\sum_{m=-M}^{M}\left[\frac{\mathrm{d}\gamma_m}{\mathrm{d}t}\mathrm{e}^{\mathrm{i}m\xi} - D_m\rho_m\mathrm{e}^{\mathrm{i}m\xi}\right] &= \left[U - \frac{\mathrm{d}X_C}{\mathrm{d}t}\right] + \boldsymbol{u}_E\cdot\boldsymbol{e}_x, \\ \frac{1}{2}\sum_{m=-M}^{M}\left[\frac{\mathrm{d}\rho_m}{\mathrm{d}t}\mathrm{e}^{\mathrm{i}m\xi} - C_m\gamma_m\mathrm{e}^{\mathrm{i}m\xi}\right] &= \boldsymbol{u}_E\cdot\boldsymbol{e}_r. \end{aligned}\right\} \tag{15}$$

The initial condition is that of a circular vortex ring in the (y, z)-plane, so that

$$R^*(\xi) + \frac{1}{2}\sum_{m=-M}^{M}\rho_m(0)\mathrm{e}^{\mathrm{i}m\xi} = R, \quad \sum_{m=-M}^{M}\gamma_m(0)\mathrm{e}^{\mathrm{i}m\xi} = 0, \tag{16a, b}$$

for all ξ.

We now assume that a timescale τ exists for oscillation of the vortex (to be determined presently), such that the products $e\tau$ and $s\tau$ are $O(\epsilon)$. If we then take

$\mathrm{d}X_C/\mathrm{d}t = U$ and substitute (14) into (15), keeping only terms of $O(\epsilon)$ and lower, we obtain a set of equations for the radial and axial displacements of the ring as

$$\left.\begin{aligned}\sum_{m=-M}^{M}[\dot{\rho}_m \mathrm{e}^{\mathrm{i}m\xi} - C_m \gamma_m \mathrm{e}^{\mathrm{i}m\xi}] &= 2eR^* \cos(2\xi)\\ \sum_{m=-M}^{M}[\dot{\gamma}_m \mathrm{e}^{\mathrm{i}m\xi} - D_m \rho_m \mathrm{e}^{\mathrm{i}m\xi}] &= 0\end{aligned}\right\} \text{in PST,} \qquad (17a)$$

$$\left.\begin{aligned}\sum_{m=-M}^{M}[\dot{\rho}_m \mathrm{e}^{\mathrm{i}m\xi} - C_m \gamma_m \mathrm{e}^{\mathrm{i}m\xi}] &= 2eR^* \cos^2(\xi)\\ \sum_{m=-M}^{M}[\dot{\gamma}_m \mathrm{e}^{\mathrm{i}m\xi} - D_m \rho_m \mathrm{e}^{\mathrm{i}m\xi}] &= -2eX_C\end{aligned}\right\} \text{in NST,} \qquad (17b)$$

$$\left.\begin{aligned}\sum_{m=-M}^{M}[\dot{\rho}_m \mathrm{e}^{\mathrm{i}m\xi} - C_m \gamma_m \mathrm{e}^{\mathrm{i}m\xi}] &= sR^* \sin(2\xi)\\ \sum_{m=-M}^{M}[\dot{\gamma}_m \mathrm{e}^{\mathrm{i}m\xi} - D_m \rho_m \mathrm{e}^{\mathrm{i}m\xi}] &= 0\end{aligned}\right\} \text{in PSH,} \qquad (17c)$$

$$\left.\begin{aligned}\sum_{m=-M}^{M}[\dot{\rho}_m \mathrm{e}^{\mathrm{i}m\xi} - C_m \gamma_m \mathrm{e}^{\mathrm{i}m\xi}] &= 0\\ \sum_{m=-M}^{M}[\dot{\gamma}_m \mathrm{e}^{\mathrm{i}m\xi} - D_m \rho_m \mathrm{e}^{\mathrm{i}m\xi}] &= 2sR^* \cos(\xi)\end{aligned}\right\} \text{in NSH.} \qquad (17d)$$

It is noted that after multiplying the equations (17*a–d*) by the timescale τ and substituting (16) for R^*, all terms in the equations are of order ϵ except for the terms related to the difference between R^* and R, which are of order ϵ^2. For the purpose of solution of equations (17), dependence of R^* on ξ is therefore negligible to order ϵ; however, the dependence of R^* on ξ does allow us to satisfy the initial condition (16) on the radial displacement of the vortex ring, as is shown for the following specific cases.

The PST case in (17*a*) can be satisfied to $O(\epsilon)$ using only the $m = \pm 2$ modes, which gives the leading-order solution for ring displacement as

$$\left.\begin{aligned}\rho_2(t) &= \bar{\rho}_{-2}(t) = \hat{\rho}\,\mathrm{e}^{\mathrm{i}\alpha t},\\ \gamma_2(t) &= \bar{\gamma}_{-2}(t) = -eR/C_2 + (\mathrm{i}\alpha\hat{\rho}/C_2)\,\mathrm{e}^{\mathrm{i}\alpha t},\end{aligned}\right\} \qquad (18)$$

where $\hat{\rho}$ is a complex constant which must be determined by initial conditions and an overbar denotes the complex conjugate. The oscillation frequency α is given by

$$\alpha = (-C_2 D_2)^{1/2}. \qquad (19)$$

The solution (18) yields a periodic oscillation in which the ring elongates (in the $m = \pm 2$ mode) alternatively in the direction of stretch and that of compression of the external flow with a period $\tau = 2\pi/\alpha$. If we include the $O(1)$ terms in the expressions (13) for C_m and D_m, the dimensionless oscillation period τ becomes

$$\tau = 4\pi R^2[\{4\ln(R) + 4A - 0.22\}\{3\ln(R) + 3A - 2.23\}]^{-1/2}, \qquad (20)$$

which is the same period as obtained by Dhanak & Bernardinis (1981) for oscillation of elliptical vortex rings. In (20), the constant A is given by (5) in general and is equal to $\frac{1}{4}$ for uniform vorticity profile across the core. From the initial condition (16*b*), we require that

$$\gamma_2(0) = \bar{\gamma}_{-2}(0) = -eR/C_2 + \mathrm{i}\alpha\hat{\rho}/C_2 = 0, \qquad (21)$$

which gives an expression for the constant $\hat{\rho}$ as

$$\hat{\rho} = -\mathrm{i}eR/\alpha = -\mathrm{i}e\tau R/2\pi. \tag{22}$$

In order to satisfy the other initial condition (16*a*), we set the function $R^*(\xi)$ as

$$R^*(\xi) = R - \tfrac{1}{2}\rho_2(0)\,\mathrm{e}^{2\mathrm{i}\xi} - \tfrac{1}{2}\rho_{-2}(0)\,\mathrm{e}^{-2\mathrm{i}\xi} = R\left[1 - \frac{e\tau}{2\pi}\sin(2\xi)\right]. \tag{23}$$

We note that $\max(R^* - R) = O(e\tau)$ and $\max(\rho/R) = O(e\tau)$, as was previously assumed.

For the NST case in (17*b*), we must include both the $m = \pm 2$ and $m = 0$ modes to obtain a solution for the displacement of the ring. Recalling that $C_0 = D_1 = 0$ from (13) and using the half-angle formula $\cos(2\xi) = 2\cos^2(\xi) - 1$, a solution to (17*b*) for ρ_m and γ_m is obtained as

$$\left.\begin{aligned} &\rho_0(t) = eRt, && \gamma_0(t) = [-eU + eRD_0/2]\,t^2, \\ &\rho_2(t) = \bar{\rho}_{-2}(t) = \hat{\rho}\,\mathrm{e}^{\mathrm{i}\alpha t}, && \gamma_2(t) = \bar{\gamma}_{-2}(t) = -\frac{eR}{2C_2} + \frac{\mathrm{i}\alpha\hat{\rho}}{C_2}\mathrm{e}^{\mathrm{i}\alpha t}. \end{aligned}\right\} \tag{24}$$

Here α is the same as given in (19). The $m = \pm 2$ mode gives an oscillation with period $\tau = 2\pi/\alpha$ similar to that obtained for the PST case, but the $m = 0$ mode indicates that the ring radius will increase monotonically with time (becoming unbounded in the linear theory as $t \to \infty$). The initial condition (16*b*) can be satisfied by setting $\gamma_2(0) = \gamma_{-2}(0) = 0$, which gives an expression for $\hat{\rho}$ as

$$\hat{\rho} = -\mathrm{i}eR/2\alpha = -\mathrm{i}e\tau R/4\pi, \tag{25}$$

which is half the value obtained in (22) for PST. The initial condition (16*a*) can be satisfied by setting the function R^* as

$$R^*(\xi) = R\left[1 - \frac{e\tau}{4\pi}\sin(2\xi)\right]. \tag{26}$$

For the PSH case in (17*c*), we again consider only modes $m = \pm 2$ to obtain a solution of the form

$$\rho_2(t) = \bar{\rho}_{-2}(t) = \hat{\rho}\,\mathrm{e}^{\mathrm{i}\alpha t}, \quad \gamma_2(t) = \bar{\gamma}_{-2}(t) = \frac{\mathrm{i}sR}{2C_2} + \frac{\mathrm{i}\alpha\hat{\rho}}{C_2}\mathrm{e}^{\mathrm{i}\alpha t}, \tag{27}$$

where again α is given by (19). The solution (27) yields a periodically oscillating solution (as in the PST case). The initial condition (16*b*) gives an equation for $\hat{\rho}$ as

$$\hat{\rho} = sR/2\alpha = s\tau R/4\pi. \tag{28}$$

The other initial condition (16*a*) gives an equation for $R^*(\xi)$ as

$$R^*(\xi) = R\left[1 - \frac{s\tau}{4\pi}\cos(2\xi)\right]. \tag{29}$$

From (28)–(29), we find that $\max(R^* - R) = O(s\tau)$ and $\max(\rho/R) = O(s\tau)$, as initially assumed.

For the NSH case, a solution of (17*d*) and the initial conditions (16) is obtained with only the $m = \pm 1$ modes of the form

$$\rho_1(t) = \bar{\rho}_{-1}(t) = \tfrac{1}{2}C_1 sRt^2, \quad \gamma_1(t) = \bar{\gamma}_{-1}(t) = sRt. \tag{30}$$

In obtaining (30), we have noted that $D_1 = 0$. The solution (30) indicates that the ring is tilted by the shear flow about the z-axis. The solution will break down at long time (since ρ_1 and γ_1 become unbounded as $t \to \infty$).

4. Vortex ring in an in-plane straining flow (PST)

The numerical procedure described in §2 is used in this section to solve for the nonlinear evolution of an initially circular vortex ring subject to an external in-plane straining flow. The ring evolution is found to fall into either of two categories depending on the value of the product $e\tau$. These categories are illustrated in figure 3, which shows plots of the variation with time of the aspect ratio of a projection of the ring in the (y, z)-plane for an initial ring radius $R = 10$. In figure 3(*a*), for a strain rate $e = 0.02$, we observe that the ring aspect ratio varies periodically and alternately oscillates above and below unity, which is indicative of a motion in which the ring alternately elongates in the directions of stretching and compression of the external flow. The other type of motion is illustrated in figure 3(*b*), for a higher strain rate $e = 0.05$, which shows the aspect ratio increasing monotonically (and in fact nearly exponentially) in time, as is indicative of a ring elongating in the direction of stretching of the external flow without oscillation.

A large number of computational runs indicate that the oscillating behaviour (as in figure 3*a*) is observed whenever the product $e\tau$ is below some critical value $(e\tau)_{crit}$, which varies as a weak function of initial ring radius R (non-dimensionalized by initial core radius σ_0), where τ is the oscillation period of a nearly circular ring given by (20). When $e\tau$ is above this critical value, the ring elongates continuously in the direction of stretching of the external flow and eventually pinches off on itself. Values of $(e\tau)_{\text{crit}}$ are given for four values of R in table 1, and we see that as R is increased by a factor of four, $(e\tau)_{crit}$ decreases only by about 10%. The uncertainty of the values given in table 1, which is at most 4%, is due to restrictions on the number of runs which could be performed.

Profiles of the ring form during a cycle of oscillation (for the periodic case) are shown in figures 4 and 5 for the case $R = 10$ and $e\tau = 4.26$. In these figures, and other figures of a similar form to be shown later, a circle is drawn about each of a series of points along the core axis on the normal plane to the axis. The radius of each circle is set equal to the core radius $\sigma(\xi, t)$ of the ring at that point. Unless otherwise mentioned, circles are drawn only at every fifth computational point along the ring. In figure 4, we show plan views of the ring (looking along the x-axis) at the initial plane and at four stages of the periodic motion. The circles are viewed from the side, so they appear as line segments in figure 4(*a*). The orientation of the ring with respect to the plane of view (in this case the (y, z)-plane) can be estimated in these figures by observing the change in orientation of the small circles drawn about the core. The ring initially seems to be passively stretched by the external flow (figure 4*b*). However, after a certain amount of elongation is achieved, the self-induced motion counters the effect of the external flow and eventually reverses the minor and major axes of the ring, so that the ring becomes elongated in the direction of compression in the external flow (figure 4*d*). In figure 4(*e*), the ring has nearly returned to a circular shape with the core axis C in a plane parallel to the (y, z)-plane.

The cycle of oscillation shown in figure 4 seems very similar to that predicted by the linear theory of §3, and the oscillation period is also within about 10% of the value of τ given by (20). However, some nonlinear effects are observed, as demonstrated by the square shape of the ring projection in figure 4(*c*) and the slight deviations from a

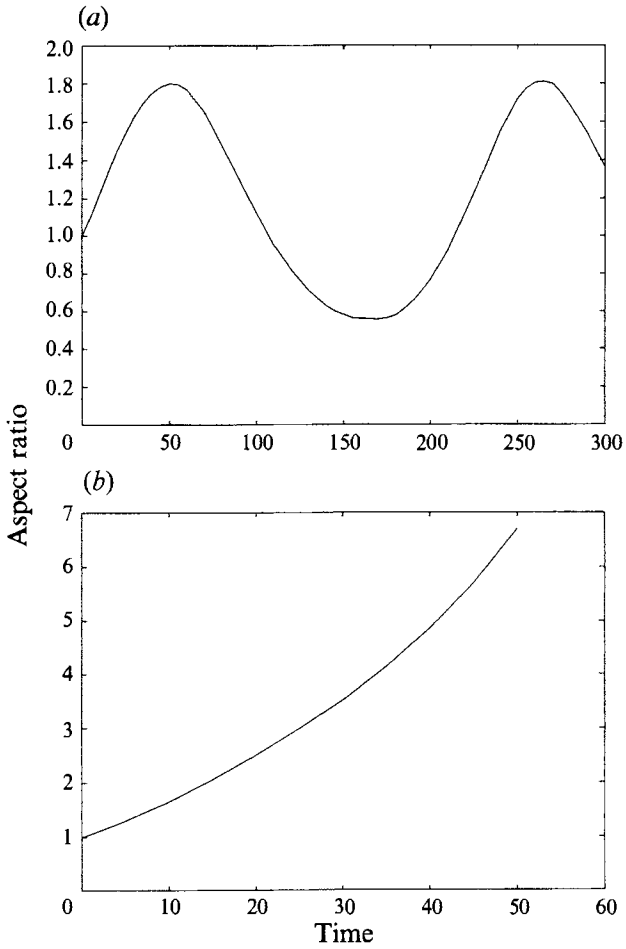

FIGURE 3. Variation with time of the aspect ratio of a projection of the ring axis in the (y, z)-plane for PST. Plots are for $R = 10$ and show (a) an oscillating ring ($e = 0.02$) and (b) an elongating ring ($e = 0.05$).

Dimensionless initial ring radius R	$(e\tau)_{crit}$
10	5.5 ± 0.1
20	5.2 ± 0.15
30	5.05 ± 0.05
40	4.9 ± 0.2

TABLE 1. Critical values of the product $e\tau$ for PST case, such that a ring will oscillate periodically for $e\tau < (e\tau)_{crit}$ and elongate until pinching off for $e\tau > (e\tau)_{crit}$

circular shape in figure 4(e). Our calculations followed the oscillation for about two cycles and seem to indicate periodic motion; however, it is not clear whether or not small effects due to nonlinear terms will build up over many oscillations to produce a gradual change in the oscillating ring. For instance, when $e\tau$ is very close to the critical value, we noticed that the mean core radius would decrease and the ring radius increase slightly during the first oscillation cycle.

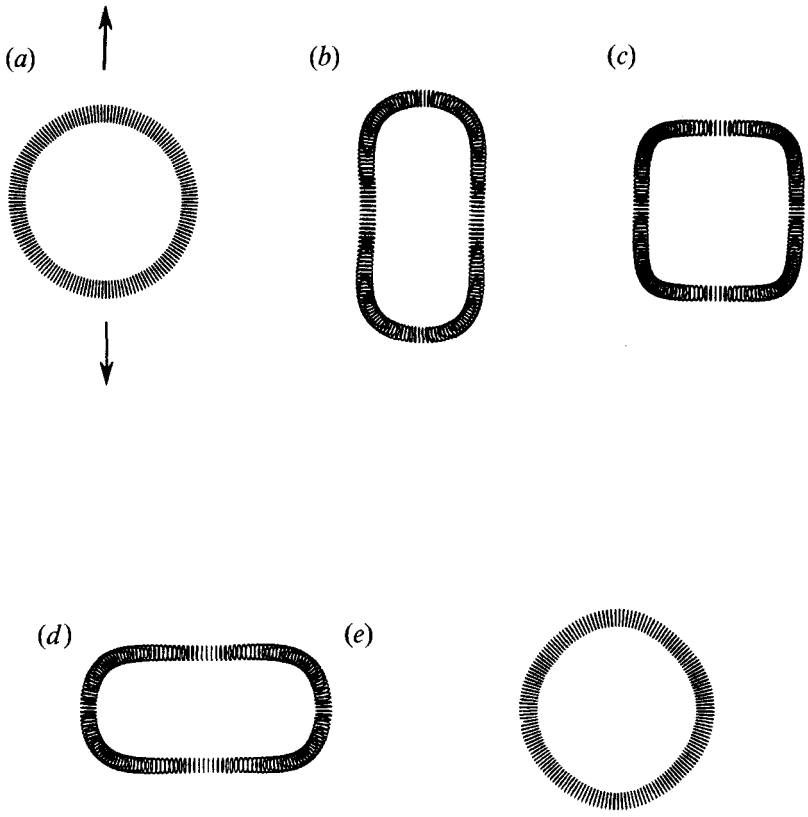

FIGURE 4. Plan view of an oscillating ring (with $R = 10$ and $e = 0.025$) in PST for different stages of the periodic motion: (*a*) initial configuration ($t = 0$), (*b*) ring elongating in direction of stretching ($t = 62.5$), (*c*) ring near half-period ($t = 125$), (*d*) ring elongating in direction of compression ($t = 187.5$) and (*e*) ring after one full period ($t = 257.5$).

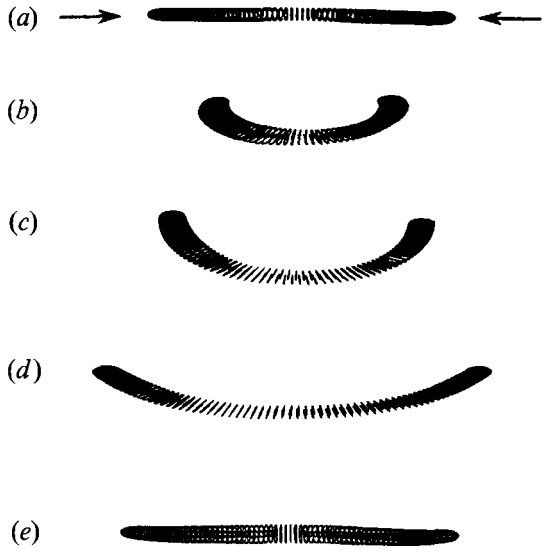

FIGURE 5. Same data as in figure 4, but showing a side view looking along the direction of stretching. The propagation direction is downward in the figure. The ring attains a nearly planar shape after one full period.

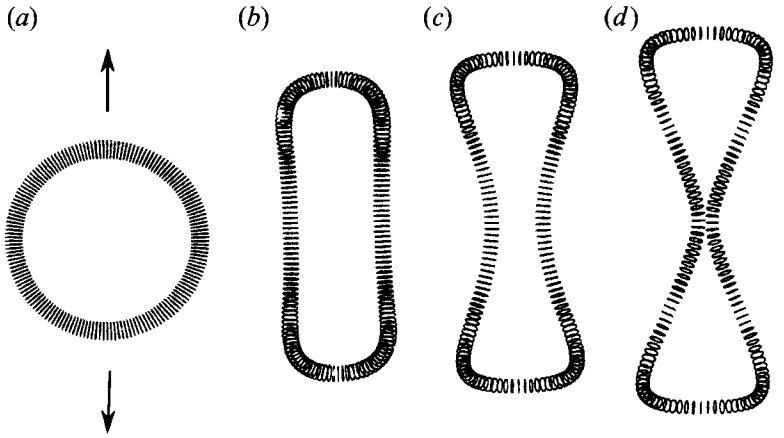

FIGURE 6. Plan view of a ring (in PST) pinching off in the centre, with stretching rate $e = 0.035$ slightly greater than the critical value 0.0325 for $R = 10$, at four different stages of the motion: (*a*) initial configuration ($t = 0$), (*b*) stretched ring with straight sides ($t = 50$), (*c*) stretched ring with concave sides ($t = 100$), and (*d*) ring at the point of pinching off ($t = 137.5$).

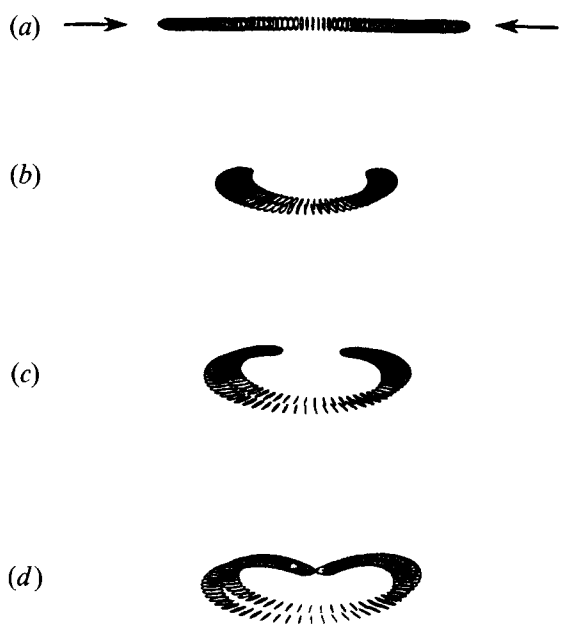

FIGURE 7. Same data as in figure 6, but showing a side view looking along the direction of stretching. The ring is propagating downward in the figure.

A side view of the oscillating ring, looking down the y-axis, is shown in figure 5 (at the same times and for the same data as in figure 4). The ring is propagating downward in the picture, and we see that the elongated sections of the ring propagate faster than the compressed sections because of their greater curvature. The switching of the axes is evident in figure 5(*d*) by the elongation of the ring in the z-direction. In figure 5(*e*), we see that the ring returns to a nearly planar shape after one cycle of oscillation.

A case showing evolution of a ring with $R = 10$ and $e\tau = 5.97$, which is just slightly greater than the critical value $(e\tau)_{crit} = 5.5$ in table 1, is plotted from a plan view (looking along the x-axis) in figure 6 and from a side view (looking along the y-axis) in figure 7. The ring is observed to elongate continuously in the direction of stretching

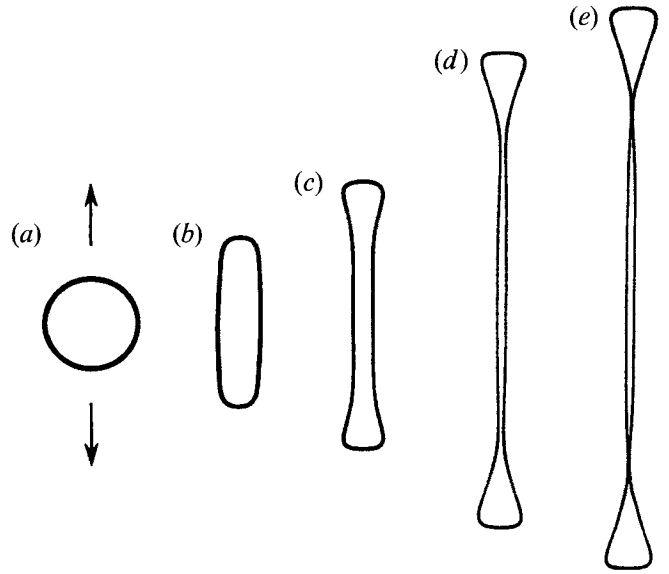

FIGURE 8. Plan view of a ring (in PST) with $R = 20$ and stretching rate $e = 0.020$ which is much larger than the critical value 0.010, showing development of an elongated centre section: (*a*) initial configuration ($t = 0$), (*b*) stretched ring with nearly straight sides ($t = 80$), (*c*) ring with concave sides ($t = 160$), (*d*) ring with 'heads' at the ends and a thin, elongated vortex pair in the centre section ($t = 240$), and (*e*) ring pinching off at two points located just behind each 'head' ($t = 270$). Every computational point is plotted in figures 8 and 9.

of the external flow, and the more strongly curved part at the ends of the elongated sections again propagates faster than the straighter central sections. In figure 6(*c*), we observe that the elongated central sections become concave inwards, which leads to pinching off in figures 6(*d*) and 7(*d*). The pinching off occurs in the ring centre and somewhat resembles that observed by Dhanak & Bernardinis (1981) for elliptical rings with aspect ratio less than about 0.2; however, we note that for initially elliptical rings the pinching off occurs after one oscillation (i.e. along what is initially the minor axis) whereas in the present case the vortex is simply elongated by external stretching and pinches off along the elongated section. Although the model which we are using for these computations does not remain valid right up to the time at which the filaments touch, the computations suggest that reconnection of the ring at the point of pinching off will produce two offspring of equal size and energy which both have ring-like (although not entirely circular) shapes.

Profiles of the ring evolution with $R = 20$ and $e\tau = 10.28$, which is about twice the critical value $(e\tau)_{crit} = 5.2$ given in table 1, are shown in figures 8 and 9 (with all computational points plotted). Figure 8 is shown from a plan view (looking down the x-axis) and figure 9 is shown from the perspective of an observer located at point $(x, y, z) = (20, 80, 0)$. The ring is observed to elongate in the direction of stretching, and in figure 8(*c*) the elongated central segments are shown to become concave. However, instead of pinching off in the middle as in figure 6, the vortex develops an elongated vortex pair in the central region and larger 'heads' on each end. The minimum separation of the two sides of the ring in figure 8(*d*) does not occur at the middle, but at two points located just behind each of the heads. In figures 9(*c*) and 9(*d*), we see that as the vortices in the central pair come closer together, the pair starts to propagate faster, and eventually overtakes the more highly curved heads at the ends of the ring.

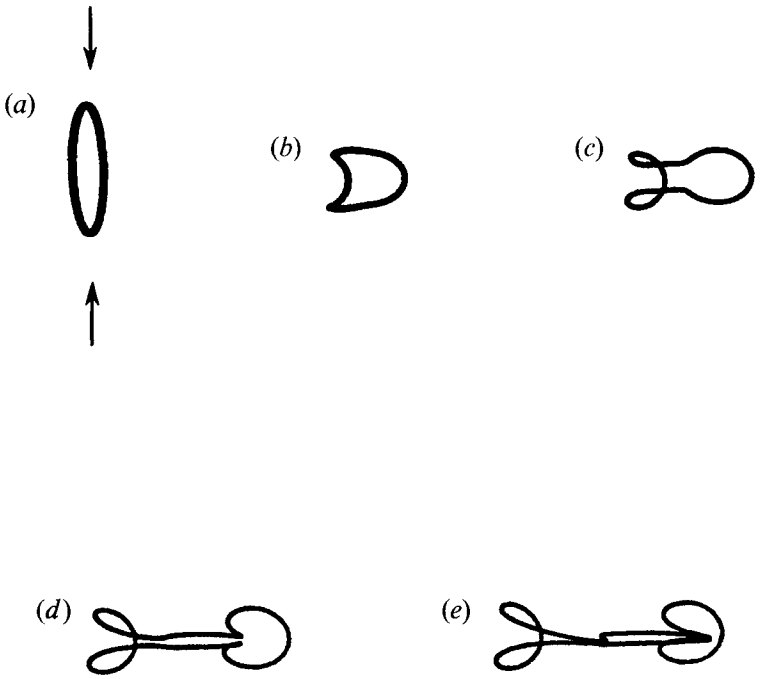

FIGURE 9. Same data as in figure 8, but with a $(x, y, z) = (20, 80, 0)$ perspective view. Ring propagates to the right in each figure. Just prior to pinching off, the elongated centre section propagates very fast and eventually out-distances the heads.

When the ring finally does pinch off in figures 8(*e*) and 9(*e*), it does so at the two points just behind the heads. From these plots, it is reasonable to assume that after reconnection, the ring breaks up to form two smaller rings of equal size and energy and one elongated vortex pair. It is not clear from these calculations, however, how the vortex pair will evolve under further stretching.

In order to explain why the elongated central vortex pair forms for high stretching rates, instead of merely pinching off at the ring centre, we recall that the mechanism leading to breakup of an elongated vortex ring is the long-range interaction between distant (and nearly parallel) parts of the vortex ring. The effect of the long-range interaction mechanism is illustrated by the well-known instability between a pair of nearly parallel vortices with opposite circulation described originally by Crow (1970) (commonly called the 'Crow instability'), which can be used to develop a rough model for pinching off of the ring in the present case. For instance, suppose that we assume that one-half of the circumference of an elongated ring determines the maximum wavelength of displacement along the two elongated sides, and that an elliptical ring will be unstable (aside from some secondary effect due to curvature at the tips of the ring) when the sides of the vortex exhibit the Crow instability at this maximum (or any smaller) wavelength. Then when the ratio of core radius σ to mean separation distance b between the opposing sides of the ring is small (i.e. $\sigma/b \ll 1$), the ring is predicted to become unstable based on Crow's analysis for aspect ratios less than about $1/2\pi$. An increase in σ/b will increase somewhat this critical aspect ratio for instability.

In figure 8 and in a number of plots to be shown in §§5–7, we find that when the vortex is stretched by the external flow it can be elongated without pinching off to a point where the aspect ratio is considerably less than the minimum value suggested by Crow's analysis. This observation is explained by the analysis of Marshall (1992), who

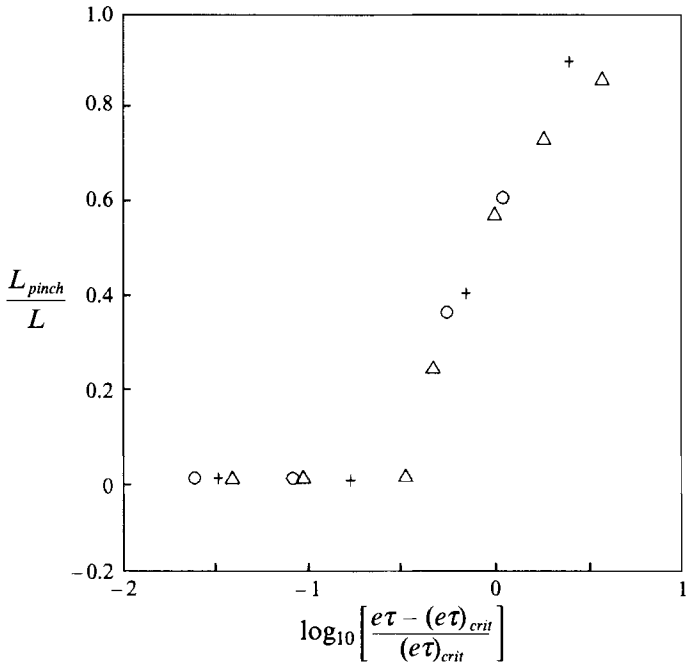

FIGURE 10. Ratio of y-coordinate L_{pinch} at the pinching-off point to the y-coordinate L at the ring tip at the time of pinching off versus the normalized strain rate for a ring in PST. The data are for an elongating ring ($e\tau > (e\tau)_{crit}$) and for the following values of R: ○, $R = 10$; △, $R = 20$; +, $R = 40$.

showed that an external stretching flow tends to stabilize a vortex pair to the Crow instability. From this observation, we expect that if the stretching of the ring is strong enough, the ring can be elongated indefinitely without pinching off at the centre owing to the Crow instability mechanism. The curvature at the ends of the ring does eventually cause pinching off to occur near the heads (which is due to local curvature rather than long-range interaction), but at high stretching rates this happens at very low ring aspect ratios.

The offspring of the ring after breakup are characterized by the length of the central vortex pair (if one is formed), by the effective radius of the 'heads' and by the core radius. The computational results indicate that stretched rings exhibit a sort of self-similarity in the course of breaking up; in particular, when certain ratios involving these quantities are plotted as functions of $e\tau/(e\tau)_{crit}$, the results seem to be independent of the initial ring radius R. Let us denote by L_{pinch} the absolute value of the y-coordinate of the point at which pinching off first occurs (i.e. the half-length of the vortex pair) and by L the y-coordinate at the ring tip at the time of pinching off. Further, denote by R_{head} the maximum z-coordinate of any point on the ring (i.e. the half-width of the head) and by σ_{pinch} the mean core radius at the time of pinching off. A plot of L_{pinch}/L versus $\log_{10}[e\tau/(e\tau)_{crit} - 1]$ is given in figure 10 for a series of runs performed with $R = 10$, 20 and 40. As noted previously, the data in figure 10 seems to fall nearly onto one curve. It is observed in figure 10 that L_{pinch}/L equals zero for $e\tau$ less than about 1.32 times $(e\tau)_{crit}$, where the critical $e\tau$ is given in table 1, which corresponds to a run where the ring pinches off in the middle as shown in figures 6 and 7. For runs with $e\tau > 1.32(e\tau)_{crit}$, the value of L_{pinch}/L increases fairly rapidly to nearly unity, which corresponds to the formation of an elongated vortex pair in the central region as shown in figures 8 and 9.

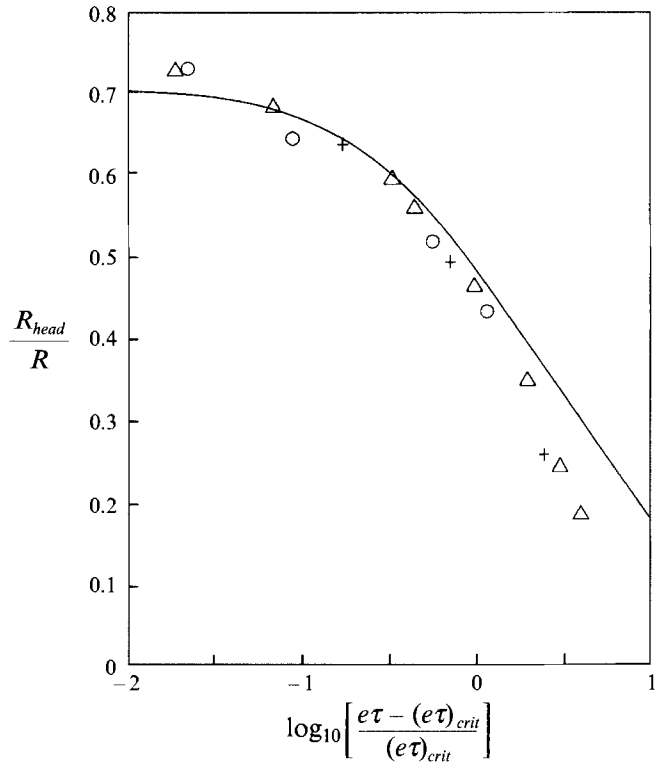

FIGURE 11. Ratio of maximum z displacement R_{head} of the ring at the time of pinching off to the initial ring radius R versus the normalized strain rate for a ring in PST. Symbols have the same meaning as in figure 10. The solid curve is the theoretical prediction from (31).

The ratio R_{head}/R is plotted versus $\log_{10}[e\tau/(e\tau)_{crit} - 1]$ in figure 11, and again the results seem to fall onto a single curve for $R = 10$, 20 and 40. The plot indicates that the radius of the offspring vortex rings, which form from the heads after reconnection of the ring, decreases as the strain rate increases for any given R. The core radius σ_{pinch} at the pinching off point (non-dimensionalized by the initial core radius σ_0) is plotted versus $[e\tau/(e\tau)_{crit} - 1]$ in figure 12. The data points again seem to be tracing nearly the same curve for $R = 10$, 20 and 40, although there seems to be more scatter in this case. We find that the mean core radius at pinching off decreases as the straining rate increases, as might have been expected.

An explanation for the observed self-similar behaviour at breakup of the ring is given in terms of the following simple model. We note that the magnitude u of the induced velocity resulting from the tip of the vortex at any point on the vortex axis C varies as a function of distance s from the tip approximately as $u = 1/s$ (in terms of the present dimensionless variables). This induced velocity from the tip causes a curvature κ of the elongated section of the vortex, which increases with time approximately as $d\kappa/dt \approx \partial^2 u/\partial s^2 = 2/s^3$. On the other hand, the stretching (at a rate e) of the vortex causes a decrease in curvature of the elongated sections at a rate $d\kappa/dt \approx -e\kappa$. When the rate of increase in curvature due to the tip induced velocity exceeds the decrease in curvature due to vortex stretching, the curvature of the elongated sections of the ring will increase in time. The self-induced velocity of the elongated sections due to this curvature causes them to come together and eventually to pinch off.

From this argument, pinching off near the tips would be expected to occur first at

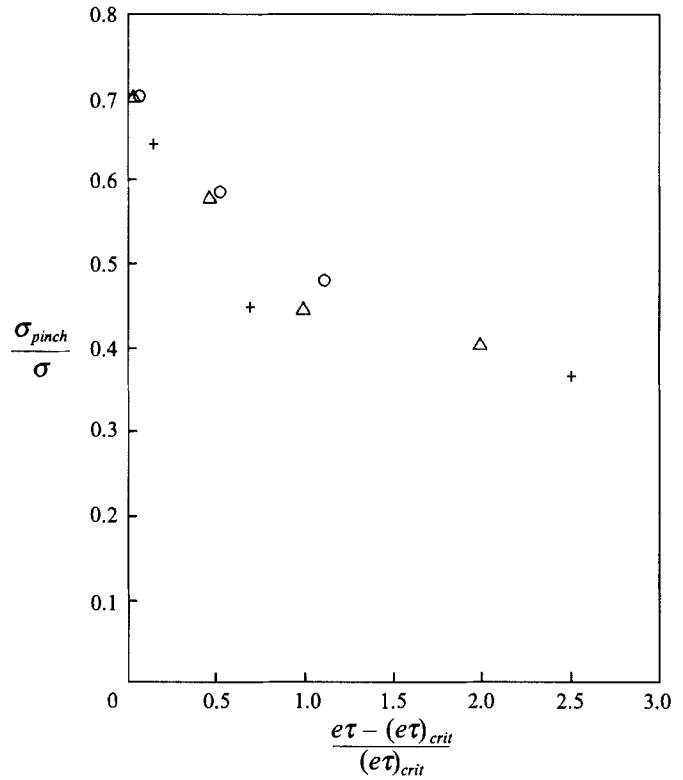

FIGURE 12. Dimensionless mean core radius σ_{pinch} of the ring at the time of pinching off versus the normalized strain rate for a ring in PST. Symbols have the same meaning as in figure 10.

a distance $s = R_{head} \leqslant (2/e)^{1/2}$ from the vortex tip, where we set $\kappa = 1/R_{head}$. Recalling the expression (20) for τ, and noting that $(e\tau)_{crit}$ in table 1 and the expression in brackets in (20) depend only weakly on R, this criterion can be written as

$$\frac{R_{head}}{R} \geqslant C\left(\frac{8\pi}{1+10^f}\right)^{1/2}, \tag{31}$$

where $f = \log_{10}[-1+e\tau/(e\tau)_{crit}]$ and C is a weak function of R given by $C^2 = \tau/[4\pi R^2(e\tau)_{crit}]$. For R between 10 and 40, our results indicate a mean value of C of 0.14, with about 10% variation about this value depending on the value of R. The prediction of the criterion (31) with $C = 0.14$ is plotted as a solid curve in figure 11, and is found to compare well with the computational results. Considering the crudeness of the arguments used to obtain (31), this agreement gives us confidence that the basic mechanism described above leading to the self-similarity in ring breakup is correct. It is noted that the basic mechanism leading to the criterion $R_{head} \leqslant (1/e)^{1/2}$ does not depend on the vortex forming a ring, and would apply also to breakup of other structures such as stretched hairpin vortices.

5. Vortex ring in a normal straining flow (NST)

For a vortex ring subject to a normal straining flow, with compression along the x-axis, profiles of the ring evolution are shown from a plan view (looking along the x-axis) in figures 13 and 14 for a ring with initial radius $R = 10$ and with two different

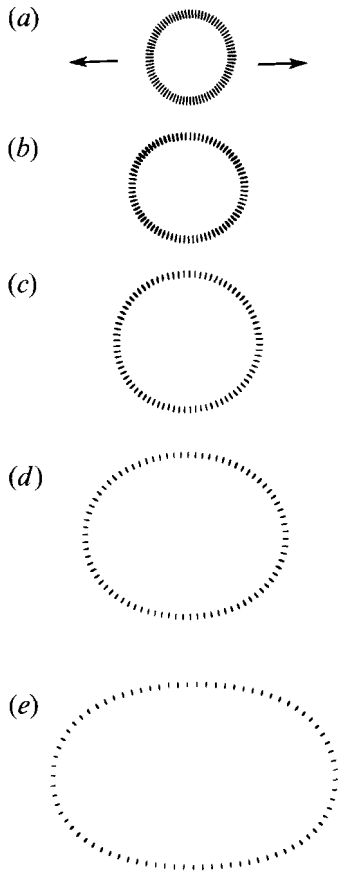

FIGURE 13. Plan view of a ring in NST with initial radius $R = 10$ and strain rate $e = 0.01$. The ring radius is observed to increase with time, keeping a nearly circular shape, until at large times it elongates in the direction of stretching. (*a*) $t = 0$; (*b*) $t = 100$; (*c*) $t = 200$; (*d*) $t = 300$, (*e*) $t = 400$.

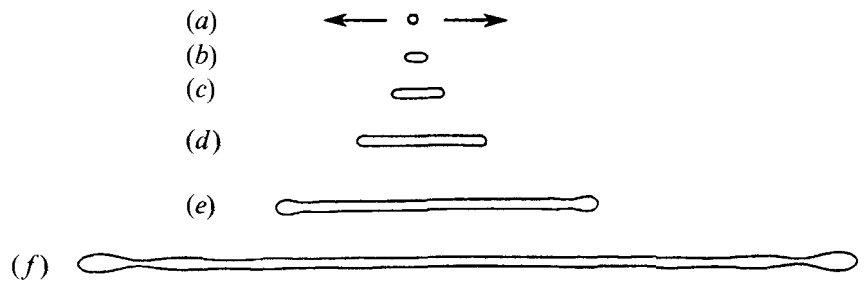

FIGURE 14. Plan view of the axis of a ring in NST with $R = 10$ but with strain rate $e = 0.05$ which is higher than that in figure 13. The ring stretches by an enormous amount without pinching off. When the ring finally does pinch off, the total vortex length, from tip to tip, is over 2500. Pinching off occurs near the 'heads' of the ring and the separation of the vortex pair in the centre section stays fairly constant in time. (*a*) $t = 0$, (*b*) $t = 50$, (*c*) $t = 100$, (*d*) $t = 150$, (*e*) $t = 200$, (*f*) $t = 250$.

values of the strain rate. In figure 13, with strain rate $e = 0.01$, the ring radius is observed to increase with time until a point is reached at which it begins elongating in the direction of stretching (figure 13*e*). The increase of ring radius agrees with the qualitative behaviour predicted for the NST case by the linear theory of §3, even though the value of $e\tau \approx 1.7$ is not small compared to unity.

The plots in figure 14 are for a strain rate $e = 0.05$ which is much higher than in the calculations shown in figure 13. Only the axis of the ring is plotted, and the thickness of the curve is not representative of the core radius. We see that for this high straining rate, the ring immediately starts elongating in the direction of stretching of the external flow. The separation distance between the elongated sides of the ring seems to remain nearly constant at the initial value ($b \approx 2R$), and even after enormous elongation there seems to be no inclination for the ring to pinch off in the centre section. Pinching off finally does occur near the ends of the ring, owing to the effect of curvature at the tip, but only after the aspect ratio decreases to less than 0.008.

For the case in figure 14, we have that $2\sigma/b < 0.1$, so that if we ignore the effect of the external flow, the vortex pair should be unstable to the Crow instability for aspect ratios less than about 0.16. However, in the computations shown in figure 14 the aspect ratio decreases to $\frac{1}{20}$ of this value without evidence of instability in the central section. In Marshall (1992), it is shown that three parameters characterize the stability of the stretched vortex pair, which can be written for the NST case as follows: (i) $\delta/\beta = 2\sigma/b$ (where b is the separation distance between the vortex axes), (ii) $\beta = 2\pi b/\lambda$ (where λ is the perturbation wavelength) and (iii) $\epsilon = (e/2\pi)(b_0/\sigma_0)^2$ (where b_0 and σ_0 are the initial values of the vortex separation distance and core radius). For the problem shown in figure 14, we estimate that $\delta/\beta \approx 0.05$, $\beta \approx 0.05$ and $\epsilon \approx 3.18$. Generally, the larger the value of ϵ, the more resistant the vortex is to the Crow instability. For instance, a calculation in figure 2(*c*) of Marshall (1992) with $\delta/\beta = 0.3$, $\beta = 1$ and $\epsilon = 0.5$ shows an almost immediate damping of the initial perturbation of the core, whereas the Crow (1970) analysis predicts this case to be unstable.

6. Vortex ring in an in-plane shearing flow (PSH)

For a vortex ring subject to an in-plane shearing flow, we again obtain a periodically oscillating motion of the ring for sufficiently small values of the product $s\tau$, in agreement with the results of the linear theory in §3. For instance, figure 15 shows plan views (looking along the x-axis) of a ring with $R = 10$ and shearing rate $s = 0.03$. The ring is observed to first elongate at about 45° to the direction of the shear flow (which coincides with the maximum direction of stretching in the external shear flow), and then to rotate clockwise so as to become elongated nearly in the direction of the shear flow in figure 15(*c*). At a later time the ring develops an elongation at 135° to the direction of the shear flow (which corresponds with the direction of maximum compression rate of the external shear) and finally returns to a nearly circular shape in figure 15(*e*). The period of oscillation in figure 15 is just over twice the value of τ obtained from (20), and this difference is thought to be due to nonlinear effects. The ring also did not return to a perfect circle at the end of the cycle in figure 15; however, the value of $s\tau$ for this case is 5.11, which is much larger than the range $s\tau \ll 1$ covered by the linear theory.

A number of runs for rings with a variety of initial radii and in different shearing rates were run. It is found that, similar to the results for PST, a periodically oscillating solution is obtained for cases where the product $s\tau$ is less than some critical value, but an elongating solution in which the ring eventually pinches off is obtained for cases with $s\tau$ over this critical value. The critical values $(s\tau)_{crit}$ are found to depend weakly on initial ring radius R, and for any given R we find (surprisingly) that $(s\tau)_{crit}$ for the PSH case is exactly equal to the value of $(e\tau)_{crit}$ given in table 1 for the PST case.

A plan view (looking down the x-axis) of a ring with $R = 10$ and for which the product $s\tau = 8.53$ is above the critical value 5.5 from table 1 is shown in figure 16. We

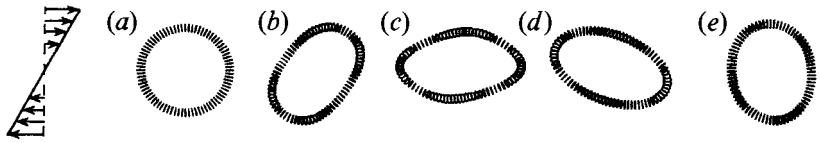

FIGURE 15. Plan view of an oscillating ring in PSH with $R = 10$ and $s = 0.03$: (*a*) initial configuration ($t = 0$), (*b*) ring elongates at about 45° to the direction of shear ($t = 50$), (*c*) ring rotates so that the elongation direction is nearly in the direction of shear flow ($t = 200$), (*d*) ring continues to rotate in a clockwise direction ($t = 300$), and (*e*) ring again adopts a nearly circular shape ($t = 400$).

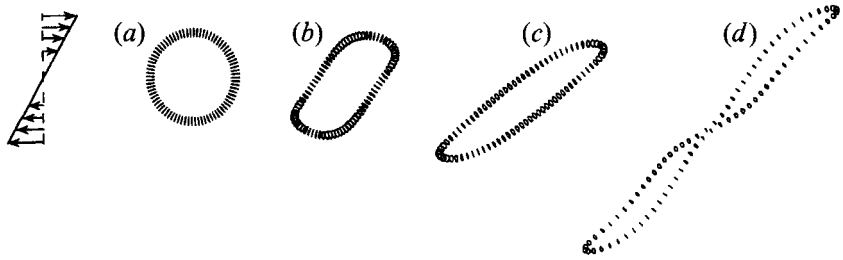

FIGURE 16. Plan view of an elongating ring in PSH with $R = 10$ and $s = 0.05$: (*a*) initial configuration ($t = 0$), (*b*) ring stretches and tilts ($t = 62.5$), (*c*) ring elongates at about 45° to the shear direction ($t = 125$) and (*d*) pinching off occurs at the ring centre ($t = 180$).

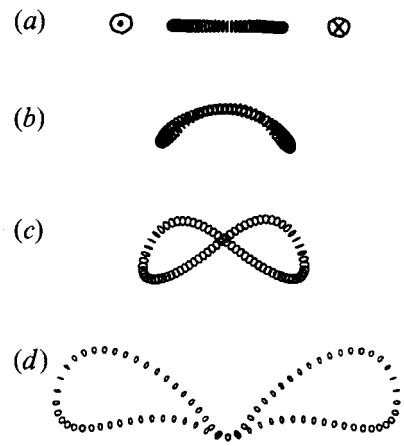

FIGURE 17. Side view of the same data as in figure 16 looking perpendicular to the direction of shear flow in the plane of the ring (i.e. along the y-axis). The ring is observed to twist before it pinches off. Propagation of the ring is downwards in the figure.

see that the ring elongates at about 45° to the direction of shear and eventually pinches off in the middle. Runs with higher shearing rates show the development of an elongated vortex pair in the ring centre, similar to the observations for PST in §4. A side view of the same data as in figure 16 is shown in figure 17, looking perpendicular to the direction of the shear flow in the plane of the ring (i.e. down the y-axis). The ring is observed to twist in figure 17(*c*) prior to the pinching off shown in figure 17(*d*).

7. Vortex ring in a normal shearing flow (NSH)

For a ring subject to a shearing flow which is initially oriented normal to the plane of the ring, the linear theory in §3 predicts that the ring will tilt with time as it is carried along by the shear flow. A side view, from the perspective of an observer at

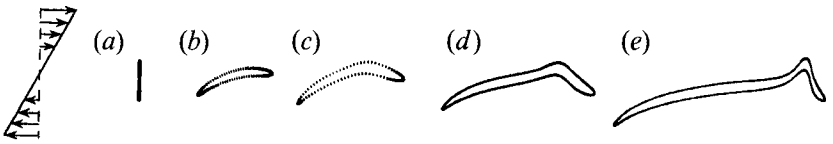

FIGURE 18. Perspective view with $(x, y, z) = (0, 40, 200)$ of the evolution of a vortex ring in NSH with $R = 10$ and $s = 0.05$, showing tilting and stretching of the ring in the direction of shear. The separation of the ring legs remain nearly equal to $2R$ in the ring centre as the ring elongates. The ring propagates downward (in the $-y$-direction) and is swept backward (in the $-x$-direction) by the shear flow (the figure is not intended to depict the relative position of the ring). The left-hand side of the ring has induced velocity which opposes the shear flow, and it seems to maintain a nearly constant orientation to the shear flow direction and stretches with time. The right-hand part of the ring has induced velocity which is in the same direction as the shear flow, so it continues to rotate in a clockwise direction. (*a*) $t = 0$; (*b*) $t = 100$; (*c*) $= 200$; (*d*) $t = 300$; (*e*) $t = 400$. All computational points are plotted for (*d*) and (*e*).

$(x, y, z) = (0, 40, 200)$, of a ring with $R = 10$ and $s = 0.05$ is shown in figure 18. The initial stages of the ring evolution (not plotted) show a clockwise tilting as would be expected from the linear theory. After considerable tilt has occurred, we note that the left-hand side of the ring (which propagates against the shear flow) becomes aligned at a nearly constant direction to the direction of shear. This left-hand side maintains this orientation and elongates with time under the stretching imposed by the shear flow, in a form which appears to be very similar to the 'hairpin' vortices that are commonly noted in turbulent shear flows. The right-hand side of the ring (which propagates in the same direction as the shear flow) does not attain a fixed orientation to the shear, but instead continues to rotate around until it is oriented nearly opposite to the original propagation direction in a hook-like shape. The ring seems to continue elongating with time in the form shown in figure 18(*e*), and no pinching off of the ring was observed.

8. Discrete vortex element simulations

In this section, the three-dimensional discrete vortex element (DVE) method of Knio & Ghoniem (1990) is used to solve for ring evolution for the case of external straining flows. The purpose of the present DVE calculations is both to demonstrate that the dumb-bell form of the vortex observed in figures 8 and 9 (with a 'head' at each end and a vortex pair in the middle) is not just an artifact of the filament method, which is not strictly valid when the filaments come very close, and to examine the effect of core instability on the vortex at very high straining rates. Shear flow cases have also been considered, but since this DVE method does not include the effect of stretching of a background vorticity field by the vortex, the calculations are subject to the same restriction $sR \ll 1$ on shear rate as stated for the filament calculations at the end of §2. For shear rates which satisfied this restriction, the results of DVE runs did not differ significantly from the filament calculations, and they are therefore not presented.

In the DVE algorithm, the vorticity field is discretized by a set of N overlapping elements whose control points are convected as material points. Each element consists of a 'blob' of vorticity, and the integral over all space of the vorticity in a given element is equal to the element amplitude $\boldsymbol{\Omega}_n$. The vorticity is distributed about the element control point according to some distribution function, which in our case was chosen to have a single lengthscale R_n called the element radius. In the current calculations, the radii of all elements are equal constants and are set such that the ratio of the typical distance between neighbouring elements and the element radius was always less than

0.5. The self-induced velocity field is obtained by substituting the discretized vorticity field into the Biot–Savart equation and integrating.

Evolution of the system requires both that the control points are convected by the self-induced and prescribed background velocity fields and that the element amplitudes are varied to account for vortex stretching. The evolution equation for element amplitude is of the form

$$\frac{\mathrm{d}\boldsymbol{\Omega}_n}{\mathrm{d}t} = \boldsymbol{\Omega}_n \cdot \nabla \boldsymbol{u}\Big|_{\boldsymbol{x}_n}, \tag{32}$$

where $\boldsymbol{u}$ denotes the total velocity field and $\nabla \boldsymbol{u}$ is evaluated at the control point $\boldsymbol{x}_n$. (Although it appears different, (32) is equivalent to the evolution equation used by Knio & Ghoniem (1990).) Since neighbouring elements overlap, we note that the vorticity at a control point $\boldsymbol{x}_n$ is not $\boldsymbol{\Omega}_n$, but is rather the contribution from all of the overlapping elements. Because of this overlap, the amplitude equation (32) does not satisfy the inviscid vorticity equation anywhere in the flow. However, it has been shown (Beale & Majda 1982) that for appropriately chosen element weighting functions, (32) converges to a solution of the inviscid vorticity equation as the number of elements increases.

Numerous tests using this algorithm have been presented by Knio & Ghoniem (1990) for steady propagation of vortex rings and growth rate of the Widnall instability on a vortex ring which give results quite close to predictions by filament methods. We have subjected the algorithm to various other tests, such as calculation of the motion of an elliptical vortex ring and the vortex core instability of Moore & Saffman (1971), in which it is again found to give predictions close to theoretical results. The calculations are also found to preserve the ring circulation to within one place in 10^4, which indicates that the calculations are almost entirely free of numerical dissipation.

A second-order predictor–corrector method was used to advance the solution in time in the DVE calculations. The computations were performed with 2000–8000 elements, with new elements being formed by element division as the computation progressed. In the initial configuration for the DVE computations, we used 17 elements to span the vortex core in each 'row' and the initial number of rows was set to either 100 (for $R = 3$) or 200 (for $R = 5$).

We first consider evolution of a ring in PST with initial ring radius $R = 5$. (This fairly small value of ring radius was chosen to reduce the number of elements required to resolve the vortex core.) Computations were performed with the DVE method for $e\tau$ much less than the critical value (estimated from table 1), and an oscillating ring motion was observed to form which appeared quite similar to that shown in §4 with the single filament computations. A plan view of a series of profiles of the ring for a case with $e = 0.0628$ is shown in figure 19 (on the left-hand side). The location of each discrete vortex element is plotted with an arrow, and the blackened region thus shows the region occupied by the vortex core. The ring evolution in figure 19 appears to be similar in form to that shown in figure 8 using the single filament model. In particular, in figure 19(*b*) we notice the formation of 'heads' at the ring ends and an elongated vortex pair at the ring centre. A side view of the ring (looking along the z-axis) is shown on the right-hand side in figure 19, where the direction of propagation is downward. We see that the heads tend at first to propagate faster than the centre section, because of their greater curvature, but that as the vortex pair in the centre comes closer together, the centre pair speeds up and eventually out-distances the heads. In figure 19(*c*), the ring is observed to touch itself at two points just behind each head. There is also some filamentation of vorticity at the tips of the vortex in this figure, which may

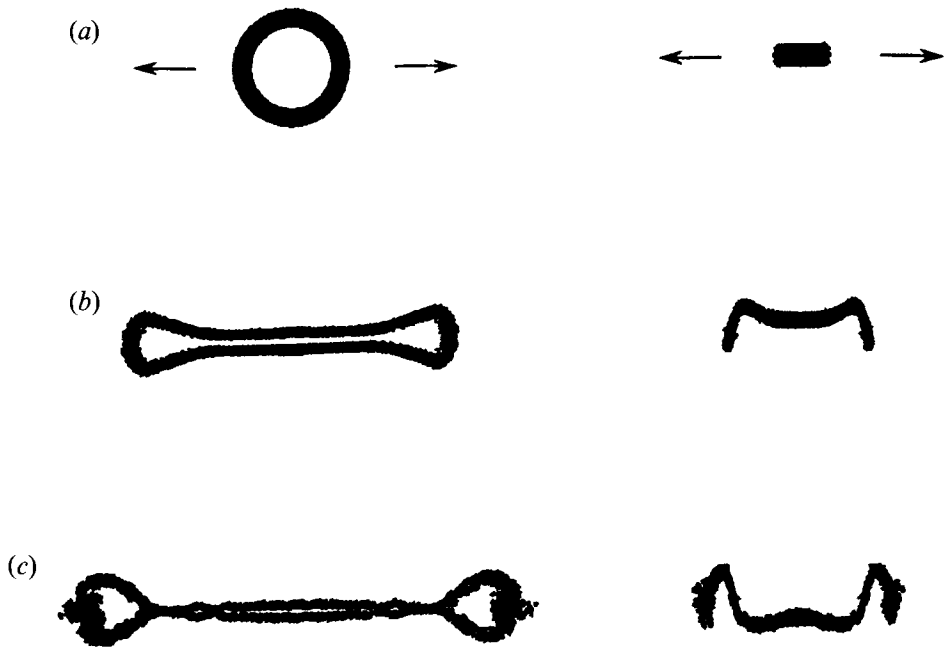

FIGURE 19. Plan view (on left-hand side of the figure) and side view looking along the z-direction (on right-hand side of the figure) of DVE calculations for a ring in PST with $R = 5$ and $e = 0.0628$. The plots show (*a*) the initial configuration ($t = 0$), (*b*) development of an elongated centre section ($t = 31.8$) and (*c*) pinching off of the core near the heads ($t = 38.9$). In the side views, the ring is propagating downward.

be due to the large amount of curvature at the tips. Of course, since the computations are based on an inviscid algorithm (with little or no numerical dissipation), we could not continue the calculations to observe the reconnection of the vortex sections.

We next consider a case in which the straining rate is sufficiently high to cause instability of the vortex core at the ends of the ring. This type of vortex core instability was suggested originally by Moore & Saffman (1971) for stationary vortices in a straining flow and extended by Kida (1981) for unsteady vortex cores for both shearing and straining flows. These two-dimensional analyses were further extended by Neu (1984) for a vortex line filament under uniform axial stretching. In terms of the dimensionless variables used in this paper, the Moore & Saffman (1971) study indicates that a vortex core subject to a plane-strain flow in its cross-sectional plane will be stable for $e < 0.30$ and unstable for $e > 0.30$. Similarly, from Kida (1981), a vortex core with a shearing flow in its cross-sectional plane will be unstable for $s > 0.207$ when s and the core axial vorticity ω are of opposite signs and for $s > 1.0$ when s and ω are of the same sign.

An example of the onset of core instability for a case with a vortex ring in an external straining flow is shown in figure 20 for a plan view (looking down the x-axis) of a ring in NST with $R = 3$ and $e = 0.628$. This value of e is greater than the critical value 0.30 for core instability. The computations show that the core flattens out in the (y, z)-plane into an elongated vortex sheet at the ends, whereas tight vortex filaments are found in the centre section. The orientation of the external straining flow is such that the ends are subject to the Moore–Saffman instability, but the filaments in the centre are not.

The results shown in this section, and others like them, lead us to conclude that the model described in §2 is at least qualitatively accurate (in the context of inviscid theory)

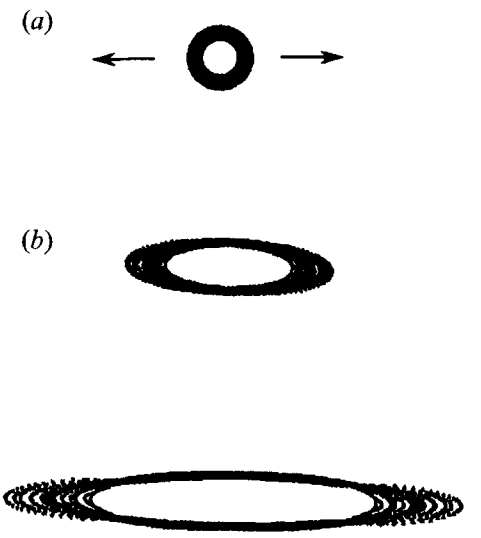

FIGURE 20. Plan view of DVE calculation for a fat ring with $R = 3$ in NST. The strain rate is $e = 0.628$, which is greater than the critical value 0.30 for onset of core instability (Moore & Saffman 1971) at the ring tips. The plots show (*a*) the initial configuration ($t = 0$), (*b*) the core is stretched by the straining flow and the ends begin to flatten out ($t = 1.91$) and (*c*) the ends flatten out into vortex sheets that continue to stretch with time ($t = 3.18$).

so long as the criteria for core instability given by Moore & Saffman (1971) and Kida (1981) are not exceeded and so long as the filaments are not actually touching. The model seems to produce reasonable results even for rather extreme cases where the radius of curvature of the ring is of the same order as the core size or where the two sides of the ring are in close proximity to each other.

9. Conclusions

This paper examines the evolution of vortex rings subject to external straining and shearing flows using a variety of theoretical and numerical approaches. The theory, which is valid for nearly circular rings and small strain and shear rates, yields periodically oscillating solutions for rings that are initially oriented in the same plane as the external straining or shearing flow (i.e. the PST and PSH cases). For a ring in a straining flow oriented such that the direction of compression is normal to the initial plane of the ring (i.e. the NST case), the linear theory indicates that the ring radius will grow monotonically with time. For a ring in a shear flow directed normal to the initial plane of the ring, the linear theory predicts that the ring will be tilted by the shear flow.

The linear theory is based on an asymptotic solution for small values of the product $e\tau$ for straining flow or $s\tau$ for shearing flow, where τ is the period of oscillation of a nearly circular ring with modes $m = \pm 2$. Numerical computations of the nonlinear evolution of the ring with both the single filament model and a three-dimensional discrete vortex element (DVE) method show that the form of solution predicted by the linear theory will still generally be observed even when $e\tau$ or $s\tau$ are not small, so long as these products are not above some critical values $(e\tau)_{crit}$ or $(s\tau)_{crit}$. Values of these critical values of $e\tau$ and $s\tau$ are obtained and are shown to be only very weakly dependent on initial ring radius R (non-dimensionalized by initial core radius σ_0).

The PST and PSH cases exhibit elongation of the ring and pinching off when $e\tau$ and $s\tau$ are above their critical values. This pinching off may occur either in a single location

at the ring centre, for $e\tau$ in the interval $1 < e\tau/(e\tau)_{crit} < 1.32$, or in two locations near the ends of the ring just behind the 'heads' for $e\tau$ above this range. In the latter case, an elongated vortex pair is formed in the central section of the ring. The DVE calculations show that at some finite time the two vortices making up this pair will be driven together by the external flow, such that the 'collapsing' or touching of the vortices in the pair occurs all along their axes nearly simultaneously rather than at isolated points (as is the case in the usual vortex reconnection problem).

The NST and NSH cases exhibit extreme elongation of the ring without pinching off. When pinching off does eventually occur in the NST case, the aspect ratio is less than 0.008 and the pinching off happens at two points just behind the 'heads' rather than in the centre. In the NSH case, one section of the ring becomes oriented at some constant angle to the direction of shear flow and stretches with time, in a manner very similar to the 'hairpin' eddies commonly observed in turbulent shear flows. No pinching off of the ring was observed in the computations with the NSH case, although it is possible that longer runs or runs with slightly different parameters might have produced pinching off near the tips of the ring at extremely long times. The ability of a ring to stretch to such extreme elongations when immersed in an external flow without pinching off is explained by the ability of vortex stretching to suppress the Crow instability.

Using DVE computations, it is shown that a section of the core which is unstable to the external straining flow will spread out into a vortex sheet. The onset of core instability and the formation of vortex sheets seems to be well predicted by the two-dimensional stability criterion of Moore & Saffman (1971).

The research of J.R.G. was supported by the US Office of Naval Research under contract number 92WX22010 and by the US Naval Undersea Warfare Center (NUWC), Division Newport. J.S.M. is grateful for a visiting position at NUWC during the summers of 1991 and 1992 through the ASEE/Navy Summer Faculty Research Program and for support from the US Army Research Office under grant number DAAL03-92-G-0277 during the final stages of the work.

REFERENCES

AREF, H. & FLINCHEM, E. P. 1984 Dynamics of a vortex filament in a shear flow. *J. Fluid Mech.* **148**, 477–497.

BEALE, J. T. & MAJDA, A. 1982 Vortex methods. I: Convergence in three dimensions. *Maths Comput.* **39**, 1–27.

BURGERS, J. M. 1948 A mathematical model illustrating the theory of turbulence. In *Advances in Applied Mechanics* (ed. R. von Mises & T. von Karman), p. 171. Academic.

CROW, S. C. 1970 Stability theory for a pair of trailing vortices. *AIAA J.* **8**, 2172–2179.

DHANAK, M. R. & DE BERNARDINIS, B. 1981 The evolution of an elliptic vortex ring. *J. Fluid Mech.* **109**, 189–216.

FRISCH, U., SULEM, P. L. & NELKIN, M. 1978 A simple dynamical model of intermittent fully developed turbulence. *J. Fluid Mech.* **87**, 719–736.

KELVIN, LORD 1880 Vibrations of a columnar vortex. *Mathematical and Physical Papers*, vol. 4, pp. 152–165. Cambridge University Press.

KIDA, S. 1981 Motion of an elliptical vortex in a uniform shear flow. *J. Phys. Soc. Japan* **50**, 3517–3520.

KIDA, S., TAKAOKA, M. & HUSSAIN, F. 1991 Collision of two vortex rings. *J. Fluid Mech.* **230**, 583–646.

KNIO, O. M. & GHONIEM, A. F. 1990 Numerical study of a three-dimensional vortex method. *J. Comput. Phys.* **86**, 75–106.

LUNDGREN, T. S. & ASHURST, W. T. 1989 Area-varying waves on curved vortex tubes with application to vortex breakdown. *J. Fluid Mech.* **200**, 283–307.

MANDELBROT, B. B. 1974 Intermittent turbulence in self-similar cascades: divergence of high moments and dimension of the carrier. *J. Fluid Mech.* **62**, 331–358.

MARSHALL, J. S. 1991 A general theory of curved vortices with circular cross-section and variable core area. *J. Fluid Mech.* **229**, 311–338.

MARSHALL, J. S. 1992 The effect of axial stretching on the three-dimensional stability of a vortex pair. *J. Fluid Mech.* **241**, 403–419.

MENEVEAU, C. & SREENIVASAN, K. R. 1987 Simple multifractal cascade model for fully developed turbulence. *Phys. Rev. Lett.* **59**, 1424–1427.

MENEVEAU, C. & SREENIVASAN, K. R. 1991 The multifractal nature of turbulent energy dissipation. *J. Fluid Mech.* **224**, 429–484.

MOORE, D. W. 1985 The interaction of a diffusing line vortex and an aligned shear flow. *Proc. R. Soc. Lond.* A **399**, 367–375.

MOORE, D. W. & SAFFMAN, P. G. 1971 Structure of a line vortex in an imposed strain. In *Aircraft Wake Turbulence and its Detection*, p. 339. Plenum.

MOORE, D. W. & SAFFMAN, P. G. 1972 The motion of a vortex filament with axial flow. *Phil. Trans. R. Soc. Lond.* A **272**, 403–429.

NEU, J. C. 1984 The dynamics of a columnar vortex in an imposed strain. *Phys. Fluids* **27**, 2397–2402.

ORSZAG, S. A. & GOTTLIEB, D. 1980 In *Approximation Methods for Navier–Stokes Problems*. Lecture Notes in Mathematics, vol. 771, pp. 381–398. Springer.

PEARSON, C. F. & ABERNATHY, F. H. 1984 Evolution of the flow field associated with a streamwise diffusing vortex. *J. Fluid Mech.* **146**, 271–283.

PEYRET, R. & TAYLOR, T. D. 1983 *Computational Methods for Fluid Flow*. Springer.

PRESS, W. H., FLANNERY, B. P., TEUKOLSKY, S. A. & VETTERLING, W. T. 1989 *Numerical Recipes (FORTRAN)*. Cambridge University Press.

PUMIR, A. & SIGGIA, E. D. 1987 Vortex dynamics and the existence of solutions to the Navier–Stokes equations. *Phys. Fluids* **30**, 1606–1626.

SHARIFF, K. & LEONARD, A. 1992 Vortex rings. *Ann. Rev. Fluid Mech.* **24**, 235–279.

WIDNALL, S. E. & SULLIVAN, J. P. 1973 On the stability of vortex rings. *Proc. R. Soc. Lond.* A **332**, 335–353.